

# The ANTARES Optical Module

## The ANTARES Collaboration

P. Amram<sup>p</sup>, M. Anghinolfi<sup>h</sup>, S. Anvar<sup>d</sup>, F.E. Ardellier-Desages<sup>d</sup>,  
 E. Aslanides<sup>b</sup>, J-J. Aubert<sup>b</sup>, R. Azoulay<sup>d</sup>, D. Bailey<sup>s</sup>, S. Basa<sup>b</sup>,  
 M. Battaglieri<sup>h</sup>, R. Bellotti<sup>e</sup>, Y. Benhammou<sup>j</sup>, F. Bernard<sup>b</sup>, R. Berthier<sup>d</sup>,  
 V. Bertin<sup>b</sup>, M. Billault<sup>b</sup>, R. Blaes<sup>j</sup>, R.W. Bland<sup>d</sup>, F. Blondeau<sup>d</sup>,  
 N. de Botton<sup>d,s</sup>, J. Boulesteix<sup>p</sup>, C.B. Brooks<sup>s</sup>, J. Brunner<sup>b</sup>, F. Cafagna<sup>e</sup>,  
 A. Calzas<sup>b</sup>, A. Capone<sup>i</sup>, L. Caponetto<sup>g</sup>, C. Cârloganu<sup>q</sup>, E. Carmona<sup>k</sup>,  
 J. Carr<sup>b</sup>, P-H. Carton<sup>d</sup>, S.L. Cartwright<sup>t</sup>, F. Cassol<sup>b</sup>, S. Cecchini<sup>f,r</sup>,  
 F. Ciacio<sup>e</sup>, M. Circella<sup>e</sup>, C. Compère<sup>l</sup>, S. Cooper<sup>s</sup>, P. Coyle<sup>b</sup>,  
 J. Croquette<sup>l</sup>, S. Cuneo<sup>h</sup>, M. Danilov<sup>o</sup>, R. van Dantzig<sup>q</sup>, C. De Marzo<sup>e</sup>,  
 R. DeVita<sup>h</sup>, P. Deck<sup>d</sup>, J-J. Destelle<sup>b</sup>, G. Dispau<sup>d</sup>, J.F. Drougou<sup>l</sup>,  
 F. Druillolle<sup>d</sup>, J. Engelen<sup>q</sup>, F. Feinstein<sup>b</sup>, D. Festy<sup>l</sup>, J. Fopma<sup>s</sup>,  
 J-M. Gallone<sup>n</sup>, G. Giacomelli<sup>f</sup>, P. Goret<sup>d</sup>, L. Gosset<sup>d</sup>, J-F. Gournay<sup>d</sup>,  
 A. Heijboer<sup>q</sup>, J.J. Hernández-Rey<sup>k</sup>, G. Herrouin<sup>l</sup>, J. R. Hubbard<sup>d</sup>,  
 M. Jaquet<sup>b</sup>, M. de Jong<sup>q</sup>, M. Karolak<sup>d</sup>, P. Kooijman<sup>q</sup>, A. Kouchner<sup>d</sup>,  
 V.A. Kudryavtsev<sup>t</sup>, D. Lachartre<sup>d</sup>, H. Lafoux<sup>d</sup>, P. Lamare<sup>d</sup>,  
 J-C. Languillat<sup>d</sup>, L. Laubier<sup>a</sup>, J-P. Laugier<sup>d</sup>, Y. Le Guen<sup>l</sup>, H. Le Provost<sup>d</sup>,  
 A. Le Van Suu<sup>b</sup>, L. Lemoine<sup>l</sup>, L. Lo Nigro<sup>g</sup>, D. Lo Presti<sup>g</sup>, S. Loucatos<sup>d</sup>,  
 F. Louis<sup>d</sup>, V. Lyashuk<sup>o</sup>, P. Magnier<sup>d</sup>, M. Marcelin<sup>p</sup>, A. Margiotta<sup>f</sup>,  
 A. Massol<sup>l</sup>, R. Masullo<sup>i</sup>, F. Mazéas<sup>l</sup>, B. Mazeau<sup>d</sup>, A. Mazure<sup>p</sup>,  
 J.E. McMillan<sup>t</sup>, J.L. Michel<sup>l</sup>, E. Migneco<sup>m</sup>, C. Millot<sup>a</sup>, P. Mols<sup>d</sup>,  
 F. Montanet<sup>b</sup>, T. Montaruli<sup>e</sup>, J.P. Morel<sup>l</sup>, L. Moscoso<sup>d</sup>, M. Musumeci<sup>m</sup>,  
 S. Navas<sup>b</sup>, E. Nezri<sup>b</sup>, G.J. Nooren<sup>q</sup>, J. Oberski<sup>q</sup>, C. Olivetto<sup>b</sup>,  
 A. Oppelt-Pohl<sup>b</sup>, N. Palanque-Delabrouille<sup>d</sup>, R. Papaleo<sup>m</sup>, P. Payre<sup>b</sup>,  
 P. Perrin<sup>d</sup>, M. Petrucetti<sup>i</sup>, C. Petta<sup>g</sup>, P. Piattelli<sup>m</sup>, J. Poinsignon<sup>d,s</sup>,  
 R. Potheau<sup>b</sup>, Y. Queinec<sup>d</sup>, C. Racca<sup>n</sup>, G. Raia<sup>m</sup>, N. Randazzo<sup>g</sup>,  
 F. Rethore<sup>b</sup>, G. Riccobene<sup>m</sup>, J-S Ricol<sup>b</sup>, M. Ripani<sup>h</sup>, V. Roca-Blay<sup>k</sup>,  
 J.F. Rolin<sup>l</sup>, A. Rostovstev<sup>o</sup>, G.V. Russo<sup>g</sup>, Y. Sacquin<sup>d</sup>, E. Salusti<sup>i</sup>,  
 J-P. Schuller<sup>d</sup>, W. Schuster<sup>s</sup>, J-P. Soirat<sup>d</sup>, O. Souvorova<sup>d,j</sup>,  
 N.J.C. Spooner<sup>t</sup>, M. Spurio<sup>f</sup>, T. Stolarczyk<sup>d</sup>, D. Stubert<sup>j</sup>, M. Taiuti<sup>h</sup>,  
 C. Tao<sup>b</sup>, Y. Tayalati<sup>d</sup>, L.F. Thompson<sup>t</sup>, S. Tilav<sup>s</sup>, R. Triay<sup>c</sup>, V. Valente<sup>i</sup>,  
 I. Varlamov<sup>o</sup>, G. Vaudaine<sup>k</sup>, P. Vernin<sup>d</sup>, P. de Witt Huberts<sup>q</sup>, E. de Wolf<sup>q</sup>,  
 V. Zakharov<sup>o</sup>, S. Zavatarelli<sup>h</sup>, J. de D. Zornoza<sup>k</sup>, J. Zúñiga<sup>k</sup>

<sup>a</sup>COM – Centre d’Océanologie de Marseille, CNRS/INSU Université de la Méditerranée Aix-Marseille II, Marseille, France

<sup>b</sup>CPPM – Centre de Physique des Particules de Marseille, CNRS/IN2P3 Université de la Méditerranée Aix-Marseille II, Marseille, France

<sup>c</sup>CPT – Centre de Physique Théorique, CNRS, Marseille, France

- <sup>d</sup>*DAPNIA - CEA/DSM, Saclay, France*
- <sup>e</sup>*Dipartimento Interateneo di Fisica e Sezione INFN, Bari, Italy*
- <sup>f</sup>*Dipartimento di Fisica dell'Università e Sezione INFN, Bologna, Italy*
- <sup>g</sup>*Dipartimento di Fisica ed Astronomia dell'Università e Sezione INFN, Catania, Italy*
- <sup>h</sup>*Dipartimento di Fisica dell'Università e Sezione INFN, Genova, Italy*
- <sup>i</sup>*Dipartimento di Fisica dell'Università "La Sapienza" e Sezione INFN, Roma, Italy*
- <sup>j</sup>*GRPHE – Université de Haute Alsace, Mulhouse, France*
- <sup>k</sup>*IFIC – Instituto de Física Corpuscular, CSIC–Universitat de València, Valencia, Spain*
- <sup>l</sup>*IFREMER, Toulon/La Seyne-sur-Mer and Brest, France*
- <sup>m</sup>*INFN – Laboratori Nazionali del Sud (LNS), Catania, Italy*
- <sup>n</sup>*IReS – CNRS/IN2P3 Université Louis Pasteur, Strasbourg, France*
- <sup>o</sup>*ITEP, Moscow, Russia*
- <sup>p</sup>*LAM – Laboratoire d'Astronomie Marseille, CNRS/INSU Université de Provence Aix-Marseille I, France*
- <sup>q</sup>*NIKHEF, Amsterdam, The Netherlands*
- <sup>r</sup>*TESRE/CNR, 40129 Bologna, Italy*
- <sup>s</sup>*University of Oxford, Department of Physics, Oxford, United Kingdom*
- <sup>t</sup>*University of Sheffield, Department of Physics and Astronomy, Sheffield, United Kingdom*

---

## Abstract

The ANTARES collaboration is building a deep sea neutrino telescope in the Mediterranean Sea. This detector will cover a sensitive area of typically 0.1 km<sup>2</sup> and will be equipped with about 1000 optical modules. Each of these optical modules consists of a large area photomultiplier and its associated electronics housed in a pressure resistant glass sphere. The design of the ANTARES optical module, which is a key element of the detector, has been finalized following extensive R&D studies and is reviewed here in detail.

*Key words:* Neutrino Astronomy, Deep Sea Detector

*PACS:* 95.55.Vj

---

## 1 Introduction

Neutrinos offer a unique opportunity to explore the Universe in depth over a wide energy range [1]. However, since neutrino fluxes at high energy ( $E_\nu > \text{TeV}$ ) are expected to be very low [2], a very large detector volume is required. A detector immersed in the sea provides a cheap and efficient method of observing high energy muon neutrinos by detecting the muon produced from a charged current interaction in the matter surrounding the detector. The muon emits Čerenkov light as it passes through the water, and this light can be detected by a three-dimensional array of optical sensors called Optical Modules (OM). The measurement of the arrival time of the Čerenkov light at each OM allows the reconstruction of the muon direction, and the amount of light collected can be used to estimate the muon energy.

The ANTARES collaboration has started the construction of a  $0.1 \text{ km}^2$  detector to be immersed at 2400 m depth in the Mediterranean Sea 40 km off the French coast ( $42^\circ 50' \text{ N}$ ,  $6^\circ 10' \text{ E}$ ). This detector will be equipped with about 1000 OMs and has been designed to be competitive with other such detectors (DUMAND [3], Baikal [4], AMANDA [5] and NESTOR [6]), notably in terms of angular resolution. To reach this goal, extensive R&D studies have been carried out during the past years in order to optimize the design of each element of the telescope, particularly its most fundamental component, the optical module. This optimization work has involved a variety of measurements, both in the laboratory and *in situ*, as well as Monte Carlo simulations. This paper gives the results of these studies and describes in detail the final design of the ANTARES optical module.

In section 2, the constraints inherent to the operation of a deep sea neutrino detector are reviewed and the specifications for the optical modules are listed. Section 3 describes the main features of the different components of the OM as well as the assembly procedure. The test set-ups and the main results of the tests performed by the collaboration during the past years are presented in section 4. Finally, section 5 deals with mass production and quality control aspects.

## 2 Constraints for a deep-sea neutrino telescope

The detection of high energy cosmic neutrinos together with the expected background sources impose particular constraints on the design of a deep undersea detector and on its basic element, the optical module.

## 2.1 Background sources

Atmospheric muons, originating from mesons which are copiously produced by the interaction of cosmic rays with the Earth's atmosphere, are the dominant source of background for a neutrino telescope based on the detection of the muons produced in neutrino interactions. Atmospheric muons are about 10 orders of magnitude more numerous at sea level than muons produced by neutrinos. Shielding the telescope against atmospheric muons is thus one of the most important considerations of the telescope design.

A straightforward way of reducing the down-going atmospheric muon flux is to immerse the telescope as deep as possible in the sea. At 2400 m, the depth chosen for the ANTARES detector, the atmospheric muon flux is already reduced by more than 4 orders of magnitude. Though significant, this is still insufficient for the measurement of down-going neutrino interactions and a more radical method is to observe only up-going muons, using the Earth itself as a natural shield. Since the material of the Earth stops all up-going atmospheric muons, the telescope is only sensitive to muons produced in neutrino interactions.

Important sources of background light come from natural radioactivity of sea water ( $^{40}\text{K}$  decays) and from the presence of bioluminescent organisms. This optical background has both continuous and burst components which have been studied in detail at the ANTARES site [7]. Though it has no significant impact on the OM design itself, it does constrain the trigger scheme as well as the data acquisition system.

The expected signal fluxes are very low, so the surface area of the detector must be as large as possible, preferably  $1 \text{ km}^2$  or more. The  $0.1 \text{ km}^2$  telescope foreseen as the first phase of the ANTARES project, despite its limited size, should provide some initial results on high energy neutrino sources.

## 2.2 The ANTARES project

The ANTARES detector, shown in figure 1, consists of a three-dimensional array of optical modules supported by flexible vertical strings anchored to the sea bottom [8]. Each OM (figure 2) contains a large area photosensor (photomultiplier) protected from the outside pressure. The detector is connected to the shore by an electro-optical cable for data transmission and power supply.

These strings are about 400 m long and separated from each other by at least 60 m. Each string is equipped with 90 OMs, grouped together in triplets at 30 storeys (figure 3) and connected to a local control module which holds the elec-

tronics for the trigger, signal digitization, slow-control and data transmission. The storeys on a given string are spaced 12 m vertically along an interconnecting electro-opto-mechanical cable. OMs at each storey are positioned with the axis of the photomultiplier tubes (PMTs) pointing outwards and inclined at 45° below the horizontal.

The strings must be flexible for deployment. Deep sea currents may modify the shape of the strings, so an accurate positioning system is required to monitor their deformation during and after deployment and to measure the position of each element with a precision better than 20 cm. Several additional instruments are needed to monitor the environmental conditions and to calibrate the detector in time and in energy.

### *2.3 Optical module requirements*

The scientific goals and the environmental constraints on the ANTARES detector described in the previous sections lead to the following global requirements for the OM:

- Light detection must be optimized. A hemispherical photomultiplier with a large photocathode surface must be used. For maximum detection efficiency, special care must be taken to ensure the best possible optical coupling between the water and the photocathode, and the influence of the Earth's magnetic field must be minimized.
- Due to the pressure at a depth of 2400 m, the photomultiplier and its associated electronics must be housed in a pressure-resistant glass sphere. The OM must withstand conditions likely to occur during sea operations (shocks, corrosion, vibrations, exposure to sunlight, etc.).
- The OM life-time should be greater than 10 years. Due to the deep-sea environment, it will be difficult and expensive to repair the detector. Therefore, the reliability of all components should be high.

## **3 The optical module**

The layout of the OM is shown in figure 4. Its main component is a large area hemispherical photomultiplier (PMT) glued in a pressure resistant glass sphere with optical gel. A  $\mu$ -metal cage is used to shield the PMT against the Earth's magnetic field. Electronics inside the OM are reduced to a minimum, namely: the PMT high voltage power supply and a LED system used for internal calibration. The specifications for all the components are described in this section as well as the main technical solutions adopted.

Table 1

Average properties of the 10" Hamamatsu photomultiplier R7081-20. The transit time spread (TTS), the peak-to-valley ratio (P/V), and the resolution  $\sigma_E/E$  are measured from the single photo-electron spectrum. The dark count (DC) rate is measured at room temperature and at 0.25 photo-electron level. Quoted values are for a nominal gain of  $5 \cdot 10^7$ .

Photocathode area	500 cm <sup>2</sup>
High Voltage	1760 V
TTS (FWHM)	2.6 ns
P/V	2.7
$\sigma_E/E$	40 %
DC rate	$\sim 1900$ Hz

### 3.1 Component description

#### 3.1.1 Photomultiplier

The reconstruction of the neutrino direction is based on the measurement of the arrival time of the Čerenkov light at each OM. Optimization studies based on computer simulations have shown that, to achieve the desired detector performance, the photomultiplier must have a large photocathode surface ( $\geq 500$  cm<sup>2</sup>), timing resolution better than 3.0 ns (FWHM), gain  $G$  greater than  $5 \cdot 10^7$  and good energy response: peak-to-valley ratio  $P/V \geq 2$  and single photo-electron resolution  $\sigma_E/E \leq 50\%$ .

Seven types of photomultipliers with various photocathode diameters from three different manufacturers have been evaluated: 8" (R5912-02), 10" (R7081-20) and 13" (R8055) from Hamamatsu<sup>1</sup>, 9" (XP1802) and 10.6" (XP1804/D2) from Photonis<sup>2</sup>, 8" (ETL9353) and 11" (D694) from Electron Tubes Ltd<sup>3</sup>. A figure of merit was evaluated for each of these products. The photomultiplier selected is the 14-stage 10" Hamamatsu photomultiplier R7081-20 (figure 5). Its main characteristics are summarized in table 1. Details of the PMT measurements will be reported separately [9].

#### 3.1.2 High-pressure container

The photomultiplier is enclosed in a glass sphere to protect it from the pressure of the surrounding water while ensuring good light transmission. The main

<sup>1</sup> Hamamatsu Photonics, 812 joko-cho, Hamamatsu city, 431-31 Japan.

<sup>2</sup> Photonis, Avenue Roger Roncier, Z.I. Beauregard B.P. 520, 19106 Brive, France.

<sup>3</sup> Electron Tubes Limited, Bury Street, Ruislip, Middlesex, HA4 7TA, England.

Table 2

Main properties of the high-pressure glass sphere.

Material	Vitrovex 8330 (low-activity borosilicate glass)
Outer diameter	432 mm
Thickness	15 mm minimum
Refractive index	1.47 ( $300 < \lambda < 600$ nm)
Transmission	>95% above 350 nm
Depth rating	6700 m

requirements for the high pressure glass sphere to be used for the OM have been identified as:

- the ability to resist high hydrostatic pressures: about 260 bars during normal operation and up to 700 bars in qualification tests;
- transparency to photons in the wavelength range 400-500 nm;
- watertightness, at both low and high pressure;
- electrical communication with the outside via a suitable watertight and pressure-resistant connection (signal output and control of the photomultiplier high voltage and LED system);
- optical matching, implying a refractive index close to that of sea water and of the PMT glass window.

The glass sphere chosen is a commercial product from Nautilus<sup>4</sup> with proven performance for deep ocean instrument housings (table 2). As shown in figure 6, the attenuation length is greater than 30 cm above 350 nm, which corresponds to a transmission of at least 95%. The sphere is fully resistant to corrosion; it is chemically, electrically and magnetically inert. Each sphere is made of two hemispherical parts, and watertightness is ensured by precise grinding of the interface plane. The lower hemisphere (facing the PMT photocathode) supports the photomultiplier and the magnetic shielding, glued in place with silicone gel. The upper part is painted black and houses a penetrator, which provides the electrical connection between the inside and the outside, and a vacuum valve, which is used to set and monitor the OM internal pressure. The vacuum valve is the only metallic part of the glass sphere: it is made of titanium to prevent any risk of corrosion.

<sup>4</sup> Nautilus Marine Service GmbH, Heferwende 3, D-28357 Bremen, Germany.

### 3.1.3 Magnetic shielding

The Earth's magnetic field modifies the electron trajectory in the PMT, especially between the photocathode and the first dynode, and degrades the uniformity of the response. At the ANTARES site, the ambient magnetic field is expected to be uniform, pointing downward at  $23^\circ$  from the vertical with an amplitude of about  $44 \mu\text{T}$ . Laboratory measurements have shown that such a magnetic field degrades the transit time spread and peak-to-valley ratio of the 10" Hamamatsu PMT operating in nominal conditions by up to 30% (depending on the orientation).

A magnetic shield is thus used to make the PMT response sufficiently homogeneous over the photocathode surface, while minimizing shadowing effects. For this purpose, a wire cage made of  $\mu$ -metal, a nickel-iron alloy with very high magnetic permeability (between 50000 and 150000) at low field strengths from Sprint Metal<sup>5</sup>, has been developed and tested.

As shown in figure 7, the cage is composed of 2 parts: a hemispherical part which covers the entire photocathode of the PMT, and a flat part consisting of a disk with a hole in its centre to allow the neck of the PMT to fit through. It is made out of  $\mu$ -metal wire (1.1 mm diameter) clamped together at the interface of the two parts. Since  $\mu$ -metal loses its properties when mechanically stressed, the cages are constructed in two steps: first the  $\mu$ -metal wires are point welded to obtain the required configuration, then the cages are cleaned and baked at  $1070^\circ\text{C}$  for 3 hours to restore the initial properties by annealing.

The pitch of the grid ( $68 \text{ mm} \times 68 \text{ mm}$ ) was chosen to minimize the loss due to its own shadow on the photocathode (less than 4%) while reducing the ambient magnetic field by more than a factor of 2.5 everywhere inside the volume of the cage. In addition, the PMT in the detector will be fixed such that the dynodes are horizontal. Assuming a vertical direction for the residual ambient field, this orientation minimizes the gain change between several orientations of the storey around the vertical.

### 3.1.4 Optical glue

The optical glue serves two purposes. It ensures an optical link between the glass sphere and the PMT photocathode, and it fixes the mechanical position of the different elements (PMT and  $\mu$ -metal cage) inside the OM.

The main requirements for the selection of the optical glue were the following:

- it should be highly transparent and have a refractive index as close as pos-

---

<sup>5</sup> Sprint Metal, Groupe Usinor, 58160 Imphy, France.



- sible to that of the glass envelope and the PMT window (to reduce Fresnel reflection);
- it should be firm enough to hold the different components together and, at the same time, sufficiently elastic to absorb shocks and vibrations during transportation and deployment, as well as to absorb the deformation of the glass sphere under pressure (a reduction of 1.2 mm in diameter at a depth of 2400 m);
  - its optical and mechanical properties should be sufficiently stable over a 10-year period.

The material chosen is a silicone rubber gel (reference SilGel 612 A/B) from Wacker<sup>6</sup>. It is a highly transparent gel which needs 4 hours to polymerize at 23°C. It offers pronounced tackiness and very good mechanical damping properties. Details of the gluing procedure, important for optimal use of this gel, are given in subsection 3.2. After polymerization, the gel has a refractive index of 1.404, and an attenuation length of about 60 cm above 400 nm, increasing with wavelength (figure 6).

### 3.1.5 High voltage system

The role of the high voltage system is to provide the PMT with all intermediate voltages necessary for correct operation. This consists of a constant focussing voltage between the photocathode and the first dynode and a variable amplification voltage to be applied between the first dynode, the intermediate dynodes and the anode. Our tests have shown that the optimal PMT response was obtained with a focusing voltage of 800 V, while the amplification voltage should vary between 500 V and 1500 V to allow for gain adjustment over a reasonable range. The main requirements of the HV system are:

- low power consumption
- high stability at constant average light flash rate
- acceptable stability and short recovery time for strong light pulses and periods of high rate
- long term reliability
- compactness

A modified version of the base integrated HV supply PHQ5912 developed by iSeg<sup>7</sup> has been chosen. The HV and the distribution for the dynodes is generated on the base itself, which makes the design compact (figure 8) and requires only low voltage supply ( $\pm 5$  V) and cabling. The Cockcroft-Walton scheme is used to reduce power consumption to less than 300 mW, a factor

<sup>6</sup> Wacker-Chemie GmbH, Hans-Seidel-Platz 4, 81737 Munich, Germany.

<sup>7</sup> iSeg Technologies Germany GmbH, Munich Airport Center, Terminalstrass Mitte 18, 85356 Munich, Germany.

Table 3

Main properties of the LED system.

Pulse rise time	$\sim 2$ ns
Overall pulse width	4.5 – 6.5 ns
Trigger-pulse jitter	$\sim 100$ ps
Trigger rate	0 to 10 kHz
Light output (per pulse)	0 to 40 pJ
Power consumption (@ 10kHz)	0.3 mW

10 reduction compared to standard DC/DC converters and passive dividers.

Voltage stability is guaranteed at the  $10^{-4}$  level. The voltages for the last 3 dynodes are actively stabilized so as to remain constant even under heavy load. The behaviour at high pulse rates has been measured to be satisfactory for our purposes (gain variation below 5% at 100 kHz). The recovery time after an intense burst of light (due, for example, to bioluminescence) is less than 0.5 s.

### 3.1.6 LED system

Each OM is equipped with a LED system used for internal calibration (especially PMT transit time calibration). The system is composed of a fast blue LED<sup>8</sup> with peak intensity around 470 nm and its pulser. The LED is glued on the back of the PMT in order to optimally illuminate the centre of the photocathode through the aluminium coating of the tube. The pulsing circuit, whose role is to deliver short current pulses (typically a few ns) is based on an original design from Kapustinsky et al. [10], adapted for use with the most recent LEDs and optimized to reduce its electrical influence on nearby circuits (figure 9). Both the pulse amplitude and the trigger frequency can be adjusted from a single control signal made of a triggering pulse superimposed on a DC level. The main properties of the pulser are summarized in table 3. The maximum light output has been measured to be of the order of  $10^8$  photons per pulse ( $\sim 40$  pJ).

### 3.1.7 Electrical connections

The electrical connection between the OM and the local control module (LCM) is made by a penetrator fixed in a hole in the glass envelope. Using a penetrator rather than a connector offers more long term reliability. The penetrator,

<sup>8</sup> HLMP-CB15 from Agilent technologies, 3500 Deer Creek Rd., Palo Alto, CA 94304, USA.

provided by Euroceanique<sup>9</sup>, has a diameter of 20 mm. The cable connecting the OM to the LCM is 1.9 m long and contains 5 shielded twisted pairs of 0.4 mm<sup>2</sup> allocated as follows:

- One for power transmission (Max. 50 V DC, 0.1 A)
- Two for the PMT signals (100 Ohms)
- One for high voltage control and monitoring (0 to 4 V)
- One for the LED trigger signal (0 to +24 V)

In order to increase the dynamic range, the PMT anode and dynode 12 (D12) signals are both sent to the LCM where they are digitized. Differential transmission is used to reduce noise, with one twisted pair connected between the anode and D14, and the other between D12 and ground.

### 3.2 OM assembly

The assembly of an OM from the components described above takes about 8 hours (including tests) and consists of several steps (figure 10):

#### 1) *Opening of the high pressure sphere*

High pressure spheres are delivered closed with an absolute internal pressure of 800 mbars. Each sphere is equipped with a small manometer so as to easily monitor the internal pressure during the assembly process. The upper hemisphere is already painted black and equipped with its penetrator. The sphere is opened by allowing air inside through the vacuum valve.

#### 2) *Cabling of the PMT base*

The PMT base is connected by soldering to the twisted pairs of the penetrator contained in the upper part of the glass sphere.

#### 3) *Mounting of the PMT and $\mu$ -metal cage*

The lower glass hemisphere is mounted on a gluing bench specifically developed (figure 11) which allows accurate (better than 1 mm) positioning of the PMT and the magnetic cage inside the glass sphere.

First, each element has to be carefully cleaned to avoid introducing impurities that could generate bubbles in the gel after polymerization. The PMT glass window and the inner surface of the sphere are cleaned using methyl alcohol at room temperature. The  $\mu$ -metal cage is immersed for 15 min in an ultrasonic bath of methyl alcohol at 40°C.

The gluing is performed in three phases:

---

<sup>9</sup> Eurocéanique, 645 rue Mayor de Montricher, 13854 Aix en Provence, France.

- First, 2 kg of silicone gel is poured into the glass hemisphere and outgassed. During this phase, many bubbles form and are evacuated, while the volume of the gel nearly doubles temporarily.
- Next, the  $\mu$ -metal cage and the photomultiplier are positioned very slowly in the gel and the ensemble is outgassed at about 1 mbar absolute to remove the bubbles. The outgassing operation is repeated three times for 3 minutes. The outgassing is limited to 9 minutes to avoid removing too much solvent.
- Finally, the gel is left to polymerize at room temperature and pressure for at least 4 hours.

#### 4) *Optical module closure*

The PMT base connected to the upper hemisphere is plugged onto the PMT and the 2 hemispheres are aligned and joined. The OM is then sealed by applying an under-pressure of 200 mbar inside the sphere and by using putty and tape externally at the joint between the two hemispheres.

## 4 OM characterization

Many tests were necessary to finalize the choice of individual components of the OM and in particular of the photomultiplier [9]. In addition, an evaluation of the overall behaviour of the OM once all components are assembled should be performed, both to verify the assembly procedure and to estimate the figure of merit of a particular design. Several test set-ups have been designed and implemented for this purpose and are presented in this section.

### 4.1 *Uniformity of the OM response*

The aim of one of these measurements is to look for possible non-uniformities in the OM response by scanning the entire sensitive area with a point-like light source. The measurement is performed in the air, with the OM located in a dark box equipped with a mechanical system allowing a focussed blue LED to scan the entire area of the photocathode automatically (figure 12). The LED always points to the center of the OM and the light spot diameter is about 1 cm at the photocathode. Non-uniformities may have several origins: asymmetrical PMT photocathode or collection efficiency, influence of the Earth magnetic field, defects (bubbles, dust) in the gel or glass sphere, etc. They might bias the detection efficiency of the telescope and they are very difficult to correct for *a posteriori*.

The OM response (in number of photo-electrons) as a function of the position of the light spot is presented in figure 13. For central illumination ( $\theta = 0^\circ$ )

the OM sees on average 13 photo-electrons and the OM response is essentially uniform up to  $\pm 25^\circ$ . At  $\theta = 40^\circ$ , the OM response drops quickly when the light spot reaches the edge of the photocathode. The peaks at  $\pm 50^\circ$  are due to the gel-air dioptré which reflects an important fraction of the light back to the photocathode at this particular angle.

#### 4.2 Absolute calibration

Absolute calibration and the determination of the overall response of the OM are carried out in the laboratory using a water tank under light conditions similar to those found in the deep-sea environment: a completely dark water volume, occasionally illuminated by flashes of Čerenkov light produced by the passage of energetic muons. The set-up consists of a light-tight cylindrical steel tank containing 2.3 m<sup>3</sup> of pure water (figure 14). Immersed in the tank about 1.2 m deep, the OM detects Čerenkov light pulses produced in the water by nearly vertical cosmic rays. Above and below the steel tank, two pairs of scintillator hodoscopes detect the passage of these particles. A trigger is formed by requiring a time coincidence on the 4 scintillator hodoscopes. Triggers are mainly due to muons with about 1 GeV energy.

The OM signal is sent to an ADC for digitization when an event trigger is received. Two pattern units are also read out and stored for each event to determine which scintillators were hit. This information is used to reconstruct the position of the muon track with respect to the centre of the OM. The two upper hodoscopes determine the entry point of the muon, and the lower hodoscopes determine the exit point. The horizontal coordinates ( $x$  and  $y$ ) of the entry and exit points are determined with a precision of about 6 cm. The distance from the muon track to the centre of the OM can be estimated with a precision of 2–3 cm.

A motor allows the OM to be rotated around a horizontal axis passing through the centre of the sphere and perpendicular to the tank's axis. This makes it possible to measure the optical module response at different angles of incidence (angle between the direction pointed by the PMT in the OM (the OM axis) and the muon track). The zenith angle  $\theta_{OM}$  of the OM axis can vary from  $0^\circ$  (OM looking up) to  $180^\circ$  (OM looking down).

Figure 15 shows the response of an OM equipped with a 10" R7081-20 Hamamatsu PMT operated at a gain of  $10^8$  as a function of  $\theta_{OM}$ . As shown in the figure, for head-on illumination of the OM by the Čerenkov cone ( $\theta_{OM} = 42^\circ$ ), the OM gives an average of 52 photo-electrons for minimum ionizing muons at 1 m. The effective angular acceptance of the OM, defined as the angular region where the OM sees more than half of the maximum signal, is  $140^\circ$  for

this head-on illumination. Figure 15 also shows that the PMT is sensitive to a wide range of incident directions, extending up to about  $120^\circ$  from its axis. This  $120^\circ$  limit was adopted for the design of the bottom part of the storey (figure 3) to minimize the shadowing.

#### 4.3 *Endurance test*

Experience has shown that an OM will undergo significant environmental stresses over its lifetime, including:

- temperature variations during storage and transportation:  $-10^\circ\text{C}$  to  $+45^\circ\text{C}$ ;
- mechanical stresses due to ground and sea transportation;
- light exposure (a maximum of  $1000\text{ W/m}^2$  continuously for 8 hours from the sun light on the boat deck);
- permanent contact with sea water during normal operation;
- an external working pressure of 256 bars, and 307 bars for 1 hour during the acceptance tests.

To check whether the OM can be subjected to all of these conditions without significant degradation, a test campaign for environmental qualification has been conducted. To ensure reproducibility, 4 identical OMs have been built and have been subjected to 3 sets of tests: climatic, mechanical, and high pressure tests (table 4). At each step of the qualification procedure, the integrity of the OM is monitored by:

- visual inspection
- measurement of the internal pressure
- high pressure tests
- measurement of the PMT response

All four OMs successfully passed these tests.

#### 4.4 *In situ tests and long term behaviour*

Since the beginning of the ANTARES project, more than 30 OMs have been built and used for deep-sea measurements for the site evaluation campaign. These OMs have been immersed for periods ranging from a few hours to more than one year [7] without a single failure. This indicates that the OM fabrication is under control and is adequate for the intended purpose.

In November 1999, a prototype line connected to the shore via an electro-optical cable was deployed 40 km of the coast of Marseilles at a depth of

Table 4  
Summary of endurance tests.

<b>Climatic tests</b>	
Cold storage	-10 <sup>0</sup> C for 72 h
Humid heat	+50 <sup>0</sup> C and 93% relative humidity for 96 h
Dry heat	+50 <sup>0</sup> C for 16 h
Thermal shocks	+50 <sup>0</sup> C in air / +15 <sup>0</sup> in water in 10 s
Sun Exposure	+50 <sup>0</sup> C and light flux of 1000 W/m <sup>2</sup>
<b>Mechanical tests</b>	
Vibrations	1 mm from 5 to 16 Hz / 1 <i>g</i> from 16 to 55 Hz
Shocks	100 half sine shocks of 15 <i>g</i> /20 ms
<b>High pressure tests</b>	
	307 bars for 1 h

1200 m. This line was equipped with 8 OMs very similar to the final OM design. The OMs were stored for nearly 2 years before immersion, part of the time outdoors with minimum protection. The line was operated for about 6 months and recovered in June 2000. All 8 OMs were tested after recovery and were found to work as expected.

Tests were also performed in situ to quantify the destructive effect of the implosion of one OM in a storey at various depths. Storeys equipped with three empty spheres, one of which had been artificially weakened, were used. The implosion pressure could be varied by grinding out a variable flat section on the outer surface. The tests showed that the damage depended on the depth, as expected. At 1900 m, the weakened sphere imploded without damaging the other two spheres or the mechanical structure of the storey. But at 2600 m, the implosion of the weakened sphere triggered the implosion of the two other spheres and significantly distorted the mechanical structure. At this depth, the amount of energy released by the implosion is estimated to be in excess of 10<sup>6</sup> Joules. Nonetheless, even when the three spheres of a storey are destroyed (the worst case), the integrity of the string itself is not affected. It has to be emphasized that the failure of a sphere is most likely to result from inappropriate handling during deployment and transportation, a risk that can be minimized by using special procedures at these stages.

## 5 Mass production and quality control

For mass production, each element of the OM is supplied fully tested and characterized by the different suppliers. Nevertheless, several measurements

are foreseen at different stages of the assembly chain to ensure the quality and reliability of the production.

Some systematic checks applied to all OMs allow the condition and basic functioning of each element to be assessed in a quick and easy way:

- the inside pressure of the glass sphere is read from its internal manometer upon reception and should be less than 900 mbars before opening;
- the photomultiplier, which has already undergone a detailed acceptance check, is tested with its final base just before gluing simply by switching the HV on and recording the signal shape at nominal gain on a digital scope;
- the elasticity of the optical glue is measured 24 hours after polymerization and should be in a predefined range (samples of each optical glue preparation are stored for future measurements);
- the photomultiplier signal shape is recorded again just after closure of the OM and should be identical to the signal shape before gluing;
- the inside pressure of the OM is measured again before storage and should be the same as that obtained after closing.

If the OM fails to pass one of these tests during assembly, it is simply left out of the production chain.

More detailed checks are made by sampling only. They will be performed on about 5% of all OMs, chosen randomly. They consist of:

- a measurement of the refractive index of the optical glue on samples of the preparation taken after polymerization;
- a high pressure test at 307 bars;
- a measurement of the OM response to short light pulses in a dedicated black box.

## 6 Conclusion

The optical module is a key component of the ANTARES detector. In view of its importance, extensive R&D studies have been carried out by the collaboration to ensure that it would not only be optimized in terms of performance, but would also be robust enough to withstand sea-operation stresses and be highly reliable so as to guarantee proper operation during the entire lifetime of the detector. The general design and the choice of components have been finalized, so that mass production of the OMs can begin.



## 7 Acknowledgements

The authors acknowledge financial support by the funding agencies, in particular: Commissariat à l'Énergie Atomique, Centre Nationale de la Recherche Scientifique, Commission Européenne (FEDER fund), Département du Var and Région Provence Alpes Côte d'Azur, City of La Seyne, France; the Ministerio de Ciencia y Tecnología, Spain (FPA2000-1788); the Instituto Nazionale di Fisica Nucleare, Italy; the Russian Foundation for Basic Research, grant no. 00-15-96584, Russia; the foundation for fundamental research on matter FOM and the national scientific research organization NWO, The Netherlands.

## References

- [1] T.K. Gaiser, F. Halzen, T. Stanev, Phys. Rep. 258(3) (1995) 173-236; F. Halzen, Phys. Rep. 333-334 (2000) 349-364, and references therein.
- [2] T.K. Gaiser, Neutrino astronomy: physics goals, detector parameters, OECD workshop Taormina, May 1997, astro-ph9707283.
- [3] DUMAND Collaboration, Nucl. Phys. Proc. Suppl. **48** (1996) 466-468.
- [4] R.I. Bagdjev et al., Nucl. Instr. Meth. **A420** (1999) 138-154.
- [5] E. Andrés et al., Astrop. Phys. **13** (2000) 1, 20.
- [6] NESTOR Collaboration, Nucl. Phys. Proc. Suppl. **97** (2001) 105-108.
- [7] P. Amram et al., ANTARES collaboration, Astrop. Phys. **13** (2000) 127-136.
- [8] E. Aslanides et al., ANTARES collaboration, A deep sea telescope for high energy neutrinos, astro-ph/9907432 and <http://antares.in2p3.fr/Publications/proposal/proposal99.html>
- [9] ANTARES collaboration, Study of large photocathode area photomultipliers as candidates for the ANTARES neutrino telescope, in preparation.
- [10] J.S. Kapustinsky et al., Nucl. Instr. Meth. **A241** (1985) 612-613.

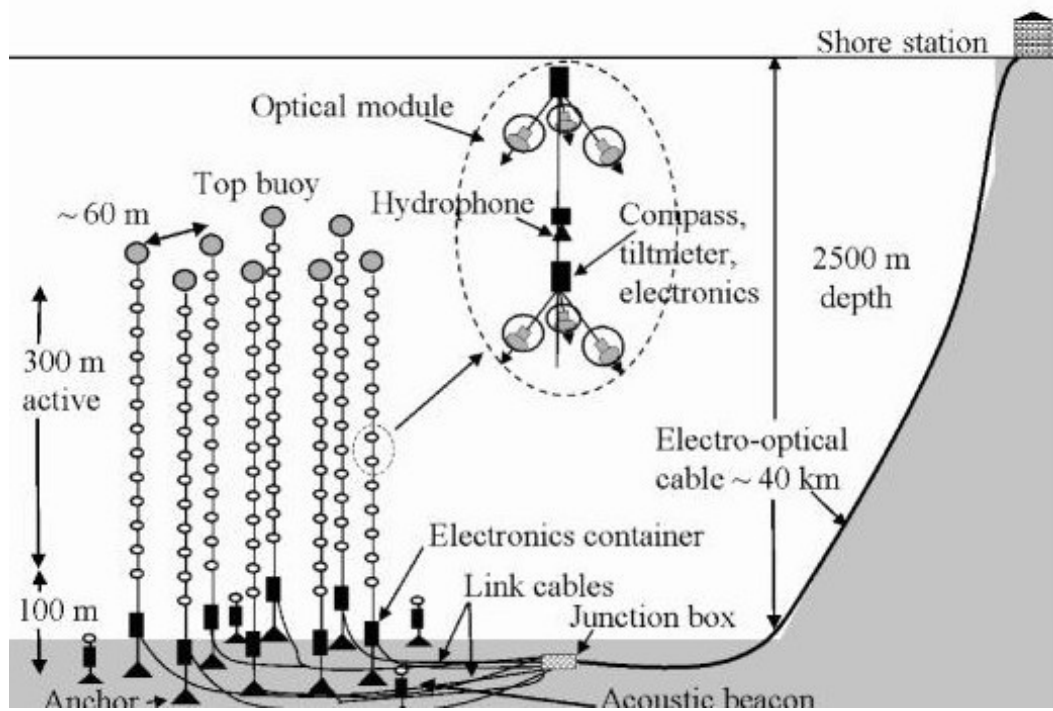


Fig. 1. Sketch of the ANTARES detector. Each string is about 400 metres long and is equipped with 90 optical modules grouped together in triplets at 30 storeys.



Fig. 2. Photograph of an optical module.

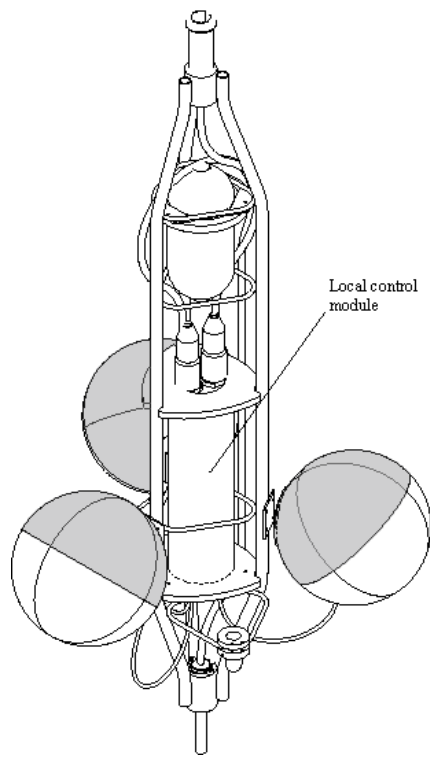


Fig. 3. Drawing of a storey equipped with 3 OMs forming a triplet. OMs are positioned with the axis of the photomultiplier tubes pointing at  $45^\circ$  below the horizontal plane. They are connected to a local control module located at the centre of the storey.

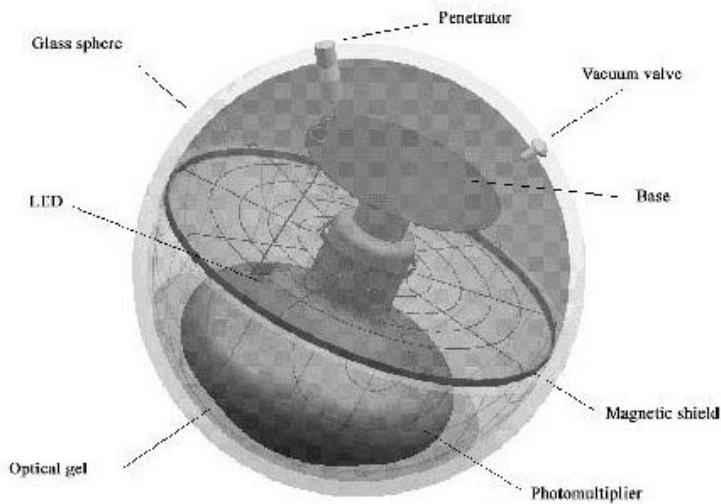


Fig. 4. Schematic 3D view of the ANTARES optical module and its components.



Fig. 5. A 10" photomultiplier model R7081-20 from Hamamatsu.

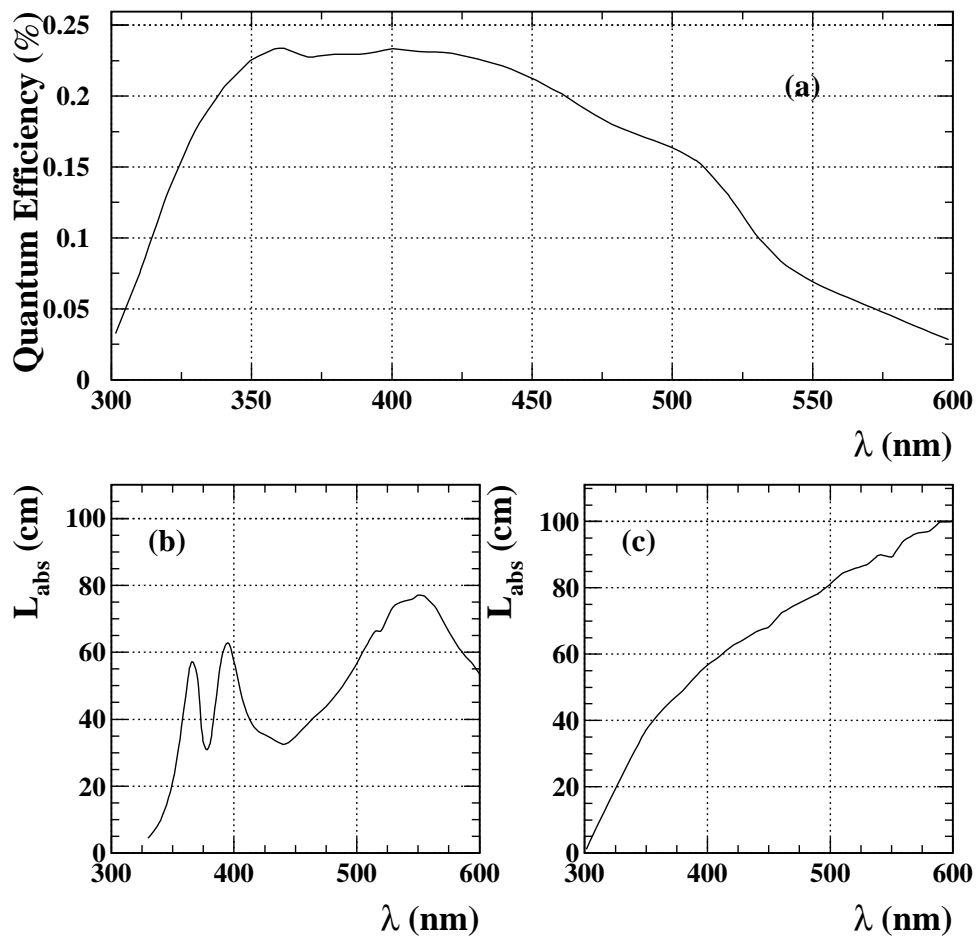


Fig. 6. (a) PMT quantum efficiency (from Hamamatsu), (b) measured absorption length of the glass sphere and (c) of the silicone gel as a function of the incident light wavelength.

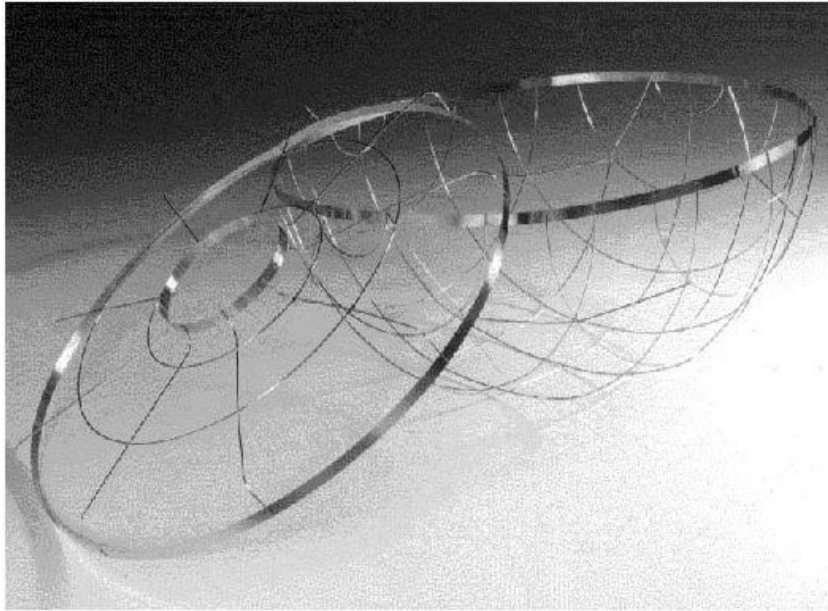


Fig. 7.  $\mu$ -metal cage for magnetic shielding. The hemispherical part has outer diameter  $\Phi=395$  mm and height  $H=199$  mm. The flat part has  $\Phi = 399$  mm,  $H=30$  mm. The two parts are linked together with four clamps of  $\mu$ -metal wire.

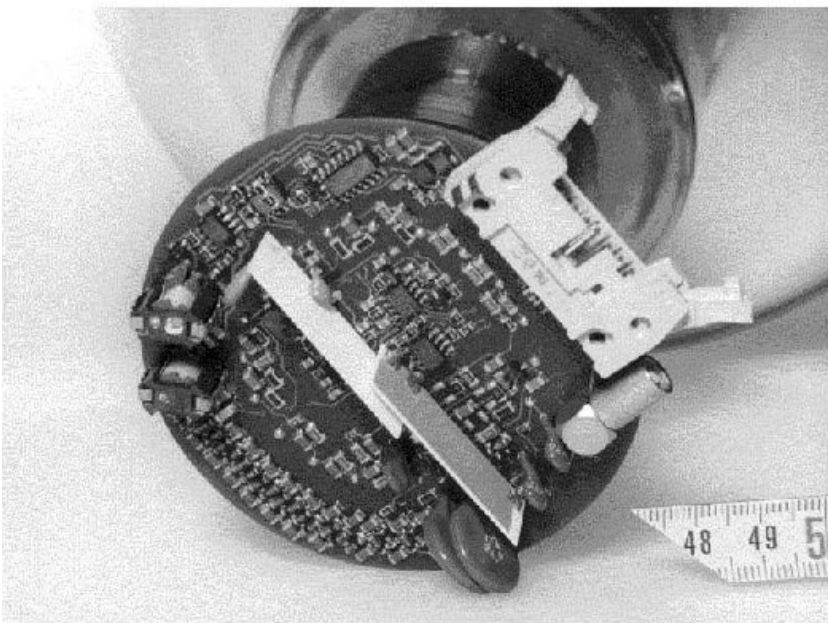


Fig. 8. PMT base with integrated high voltage power supply.

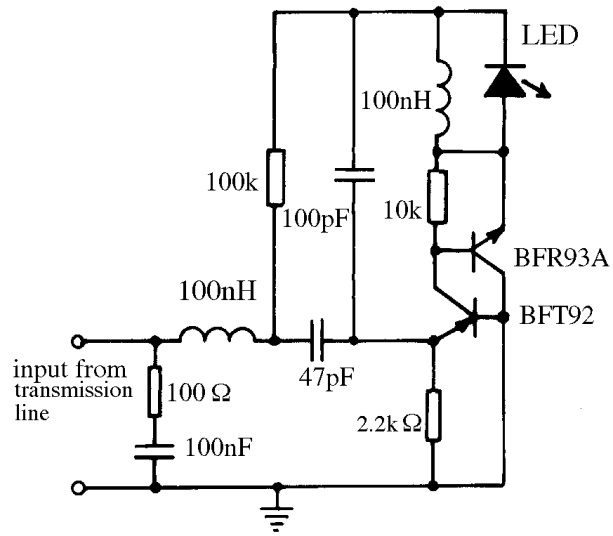


Fig. 9. LED pulsing circuit.

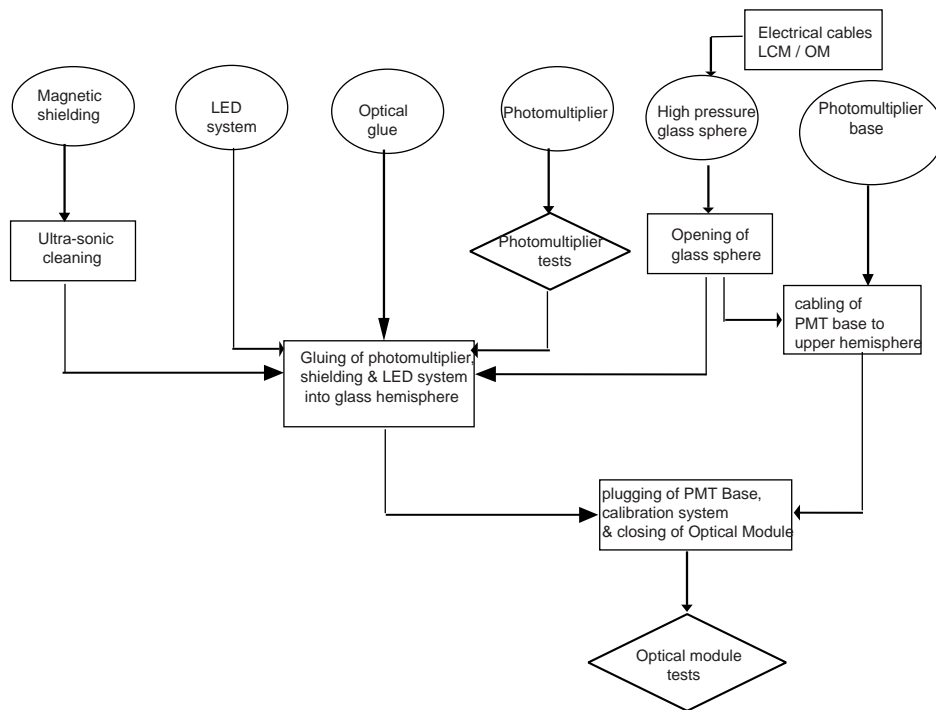


Fig. 10. OM assembly step by step.

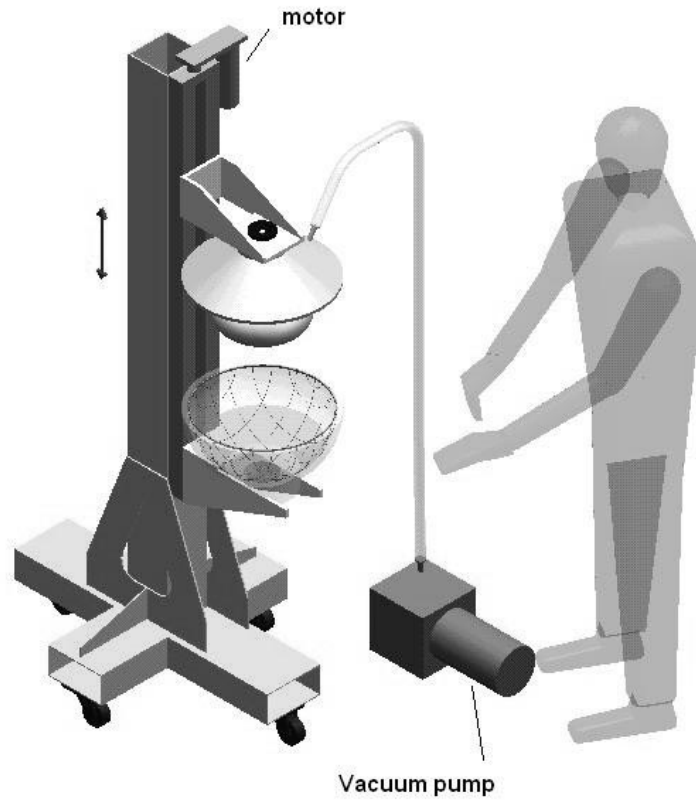


Fig. 11. Schematic 3D view of the gluing bench.

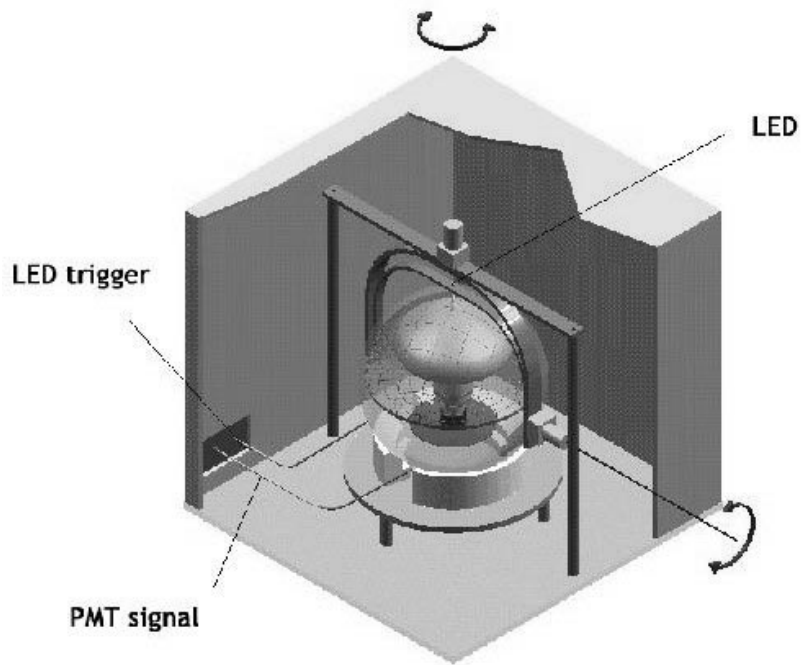


Fig. 12. Schematic view of the scanning table used to measure the uniformity of the OM response.

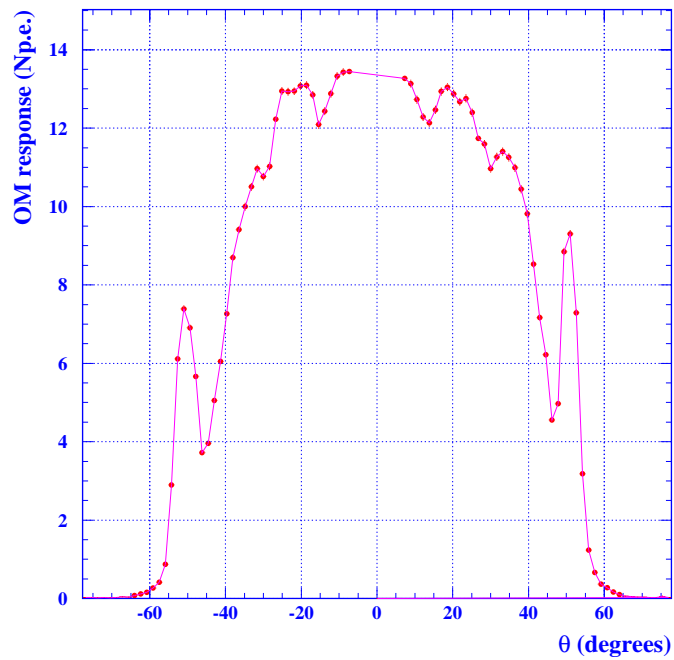


Fig. 13. Result of the measurement of the OM uniformity response as a function of the zenith angle  $\vartheta$  for an arbitrary azimuthal angle.



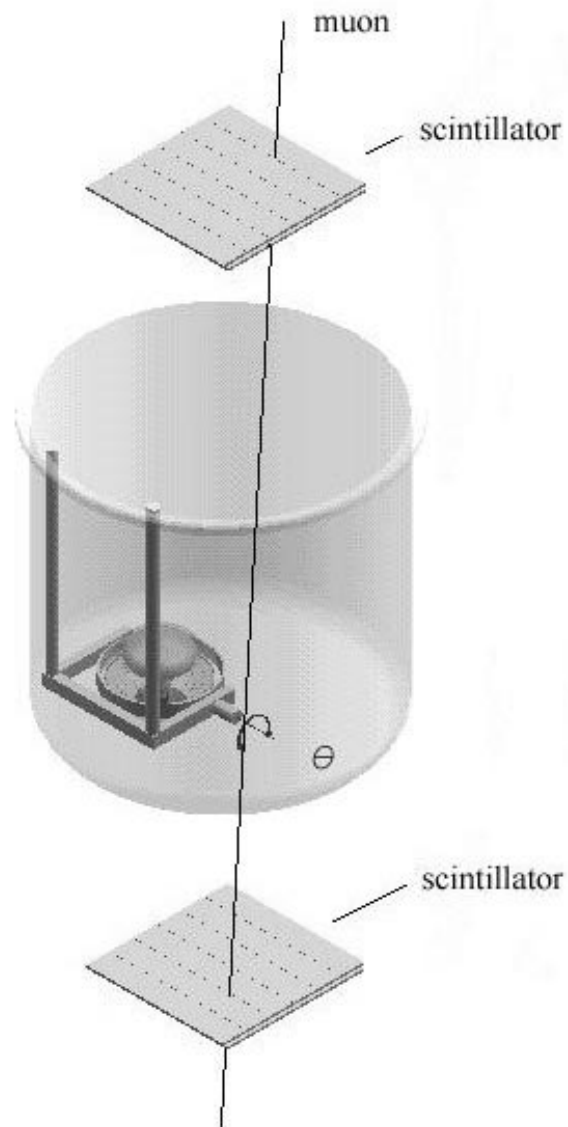


Fig. 14. Schematic view of the water tank used for absolute calibration of the OM. It is 1.5 m high, with a radius of 70 cm, and contains 2.3 m<sup>3</sup> of water kept pure by constant recycling. Above and below the tank, 3.6 m distant from each other, are two crossed scintillators plane (6 scintillator hodoscopes of 12×70 cm<sup>2</sup>).

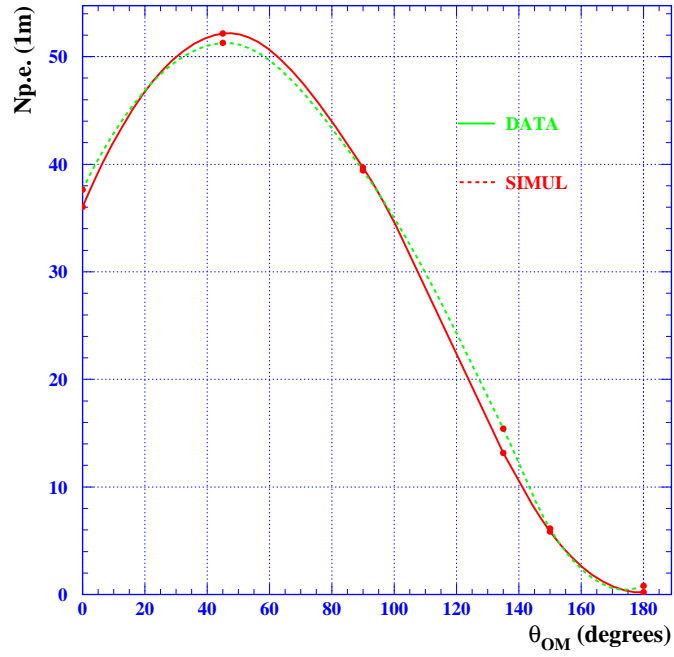


Fig. 15. Number of photo-electrons detected by the OM as a function of its zenith angle  $\theta_{OM}$  for down-going atmospheric muons at 1 m distance. Data are compared to a detailed simulation based on GEANT3.21.